JGR Oceans

RESEARCH ARTICLE
10.1029/2021JC018360

Observed Drag Coefficient Asymmetry in a Tropical Cyclone

Sheng Chen[1,2,3], Fangli Qiao[1,2,3], Jun A. Zhang[4], Yuhuan Xue[1], Hongyu Ma[1], and Siyu Chen[1]

[1]First Institute of Oceanography, Key Laboratory of Marine Sciences and Numerical Modeling, Ministry of Natural Resources, Qingdao, China, [2]Laboratory for Regional Oceanography and Numerical Modeling, Qingdao National Laboratory for Marine Science and Technology, Qingdao, China, [3]Key Laboratory of Marine Sciences and Numerical Modeling, Shandong Province, Qingdao, China, [4]NOAA's Atlantic Oceanographic and Meteorological Laboratory & University of Miami, Miami, FL, USA

Key Points:

- Momentum flux is directly observed in the right side of a tropical cyclone (TC) on an offshore platform
- Observations show that the drag coefficient is asymmetrically distributed in the right-side of the TC trajectory
- The critical wind speed for the drag coefficient saturation is approximately 20 m/s over the coastal region

Correspondence to:
F. Qiao,
qiaofl@fio.org.cn

Citation:
Chen, S., Qiao, F., Zhang, J. A., Xue, Y., Ma, H., & Chen, S. (2022). Observed drag coefficient asymmetry in a tropical cyclone. *Journal of Geophysical Research: Oceans*, *127*, e2021JC018360. https://doi.org/10.1029/2021JC018360

Received 18 DEC 2021
Accepted 2 SEP 2022

Author Contributions:
Conceptualization: Sheng Chen
Data curation: Jun A. Zhang
Formal analysis: Sheng Chen
Investigation: Sheng Chen, Yuhuan Xue, Hongyu Ma
Methodology: Sheng Chen
Supervision: Fangli Qiao, Jun A. Zhang
Validation: Fangli Qiao
Writing – original draft: Sheng Chen
Writing – review & editing: Fangli Qiao, Jun A. Zhang

Abstract The behavior of drag coefficient (C_D) in two different motion-relative quadrants of Typhoon Mujigae (2015) is investigated through the flux observations conducted on a fixed platform over the coastal region in the northern South China Sea. Observations reveal that the variation of C_D is closely related to the location relative to the tropical cyclone (TC) center. The C_D presents an enhancement when the typhoon is away from the observational site. The spatial distribution of C_D on the periphery of a TC is asymmetric, and the C_D in the right rear quadrant is much larger than that in the right front quadrant for the same wind speed range. This asymmetric distribution of C_D can be explained by the differences in wave properties between the two quadrants. C_D is smaller in cross-swell conditions than that in the along-wind wave conditions. Observations also confirm that C_D tends to level off and even attenuate with the increase of wind speed, and the critical wind speed for C_D saturation over the coastal region (~20 m/s) is much lower than that over the open ocean (~30 m/s). The observational spatial distribution of C_D in TC quadrants not only improves our understanding on the air-sea momentum flux but also provides a potential solution for the long-standing scientific bottleneck on TC intensity forecasting.

Plain Language Summary The momentum flux plays an important role in the tropical cyclone (TC) intensity change, which is typically parameterized using the drag coefficient C_D in numerical models. However, due to the lack of observations, the characteristics of C_D under TC conditions has not been well understood, especially its spatial distribution during TCs. This study investigates the behavior of C_D at different locations of TC and also compares the behavior of C_D with that in previous studies. Observational evidence shows that C_D in the right front side is much lower than that in the right rear side of a TC at the same wind speed, it presents an asymmetric distribution on the periphery of a TC. Besides, although C_D tends to saturate with the increase of wind speed over both coastal region and open ocean, the critical wind speed with C_D saturation is much lower over the coastal region (~20 m/s) than that over the open ocean (~30 m/s). The spatial distribution of C_D during TCs improves our understandings on the air-sea momentum flux, and it is recommended to be considered in TC models.

1. Introduction

Tropical cyclone (TC) is one of the severe natural disasters. Accurate forecasts for TC track and intensity are of great significance for the security of human life and property all over the world. The air-sea momentum flux, or the surface wind stress, is one of the key scientific questions in the research of ocean and atmosphere, and its accuracy of calculation affects the improvement of numerical models. It is a key factor affecting TC strength, which is crucial to accurately represent it in TC models (Bell et al., 2012; Moon et al., 2004; Sanford et al., 2011).

According to the bulk formula, the wind stress is calculated using the drag coefficient C_D and the wind speed U_{10} in the form

$$\tau = \rho_a C_D U_{10}^2 \quad (1)$$

where, ρ_a is air density. Previous observations suggested that C_D increases linearly with U_{10} when the wind speed is in the range of 5–20 m/s (Edson et al., 2013; Fairall et al., 2003; Large & Pond, 1981). However, at high wind speeds, Powell et al. (2003) found that the C_D over the ocean was saturated at U_{10} ≈33 m/s, and then the C_D attenuated with the wind speed. Since then, several studies based on laboratory experiments (Donelan

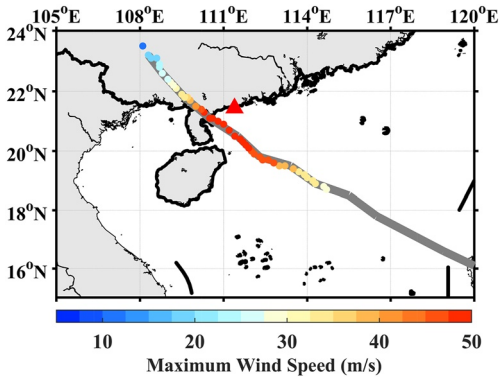

Figure 1. The best track of Typhoon Mujigae from China Meteorological Administration Tropical Cyclone Data Center; Each colored dot on the track marks tropical cyclone location every 1 hr from 12:00 a.m. on October 3rd to 12:00 a.m. on October 5th. The colors represent the maximum wind speed. BoHe observational tower's location is denoted by the red triangle.

et al., 2004; Takagaki et al., 2016), field observations (French et al., 2007; Hsu et al., 2017; Jarosz et al., 2007; Potter et al., 2015; Zhao et al., 2015), and numerical simulations (Chen, Ginis, & Hara, 2020; Moon et al., 2004; Reichl et al., 2014) confirmed the saturation and the consequent attenuation of C_D, although the critical wind speeds U_{10c} for the saturation were quite different. Holthuijsen et al. (2012) found that the U_{10c} was ~40 m/s based on the wind profiles measured by GPS drop-sondes. Bi et al. (2015) found a much smaller U_{10c} of ~18 m/s based on turbulent flux data collected on an offshore platform. It is assumed that the difference in U_{10c} is attributed to different water depths, surface wave features, sea spray, and observation methods, etc. (French et al., 2007; Jarosz et al., 2007; Powell et al., 2003; Zhao et al., 2015). High wind speeds are frequently induced by TCs, which at the same time cause complex sea state (Holthuijsen et al., 2012; Liu et al., 2017).

Black et al. (2007) analyzed 12 Scanning Radar Altimeter (SRA) spectra within ~80 km from the center of Hurricane Ivan (2004) and found that both the wave height and wavelength in the right front side of hurricane track were greater than those in the right rear side. Liu et al. (2017) investigated the spatial distribution of significant wave height during TCs through analyses of SRA images, showing that the right side of the TC track had larger wave height and rougher sea surface than the left side. These indicated an asymmetric wave state during TCs. The asymmetric wave fields during TCs may cause an asymmetric drag coefficient (Chen, Ginis, & Hara, 2020; Holthuijsen et al., 2012). Holthuijsen et al., 2012 analyzed the wind profiles collected by GPS drop sondes to show that the C_D value attenuates at $\sim 2 \times 10^{-3}$ in the right-front side of TCs, however, it levels off with a value of $\sim 5 \times 10^{-3}$ in the left front side. Additionally, the C_D values in the right front side are larger (smaller) than those in the left front side when the wind speed is less (greater) than 30 m/s. The authors attributed these to the different wave field in different sides of TCs. However, their C_D was estimated using the profile method which had large uncertainty. Chen, Ginis, and Hara (2020) also simulated the asymmetric C_D distribution, however, with no observational support.

The spatial distribution of the wind stress along the TC trajectory may lead to the spatial difference of TC intensity (Emanuel, 1995). Therefore, an improved knowledge on the spatial characteristics of the wind stress during TCs is required for better intensity forecasting (Reichl et al., 2014). While the aforementioned studies have provided certain knowledge on the complicated phenomena of C_D at high wind speeds, particularly during TCs, the spatial distribution of C_D on the periphery of a TC has not been well understood due to the lack of high-frequency field observations. In this study, the asymmetric characteristic of C_D in the right front and the right rear sides of a TC is investigated based on the momentum fluxes observed on a coastal tower in the northern South China Sea (SCS) during Typhoon Mujigae in 2015. This paper is organized as follows. Section 2 describes the experiment, platform and instrument, data and analysis method. Data analysis results and relevant discussions are presented in Section 3. This is followed by the conclusion section.

2. Data and Analysis Methods

2.1. Experiment and Method

The surface momentum fluxes were obtained from August 27th to October 6th in 2015 on the BoHe observational tower (BHOT, 21°26.5′N, 111°23.5′E) in the northern SCS. BHOT is located approximately 6.5 km from the coastline (Figure 1). The mean water depth is 16 m at the location of the tower. Where, the eddy covariance system was used to measure the fluxes. The system was installed at the end of a horizontal steel pipe that was 2.5 m long. The height of the covariance system was 17 m. This system consisted of a CSAT3A three-dimensional ultrasonic anemometer, a EC150 CO_2 and H_2O open-path gas analyzer and other sensors manufactured by Campbell Scientific, Inc.. The wind data measured by the ultrasonic anemometer with a sampling frequency of 10 Hz was used to analyze. The CSAT3A ultrasonic anemometer measures wind speed range from 0 to 60 m/s. Its measurement precision is 1 mm/s for the horizontal wind speed and 0.5 mm/s for the vertical wind speed. More detailed information of BHOT and the eddy covariance system can be referred to Chen et al. (2018, 2019), Chen, Qiao, et al. (2020).

The amplitude of wind stress τ can be calculated using the eddy covariance method as

$$\tau = \rho_a \sqrt{\langle u'w' \rangle^2 + \langle v'w' \rangle^2} = \rho_a u_*^2 \quad (2)$$

where, u', v', and $w'$are the zonal, meridional and vertical velocity fluctuations, respectively; u_* is the friction velocity; $\langle\ \rangle$ represents the Reynolds average. One hour was chosen for the Reynolds average. Quality control was made and the nonstationary motions from 1-hr turbulence data were removed following the method as in Chen et al. (2018). The wind profile under neutral condition follows the log-law

$$U(z) = \frac{u_*}{\kappa} \ln \frac{z}{z_0} \quad (3)$$

where, $U(z)$ is the mean wind speed at the height z, $\kappa = 0.4$ is the von Kármán constant, z_0 is the aerodynamic roughness length. In current situation, $z = 17$ m above the mean sea surface. Based on Equations 2 and 3, the wind speed at the typical height of 10 m U_{10} is

$$U_{10} = U(z) - \frac{u_*}{\kappa} \ln \frac{z}{10} \quad (4)$$

then, the drag coefficient C_D can be estimated through Equation 1.

2.2. Data and Analysis

In this study, the momentum fluxes observed during Typhoon Mujigae (2015) were used to estimate the drag coefficient and analyze its spatial distribution. Due to the lack of surface wave observations, the ERA5 reanalysis data were used to qualitatively present the wave field during the observational period and explain the possible linkage to the behavior of the drag coefficient with wave characteristics. Before that, ERA5 was compared with the surface wave datasets during Typhoon Rammasun (2014) to verify whether ERA5 can be used to qualitatively determine the wave situation at BHOT site.

Typhoon Mujigae formed to the east of the Philippines on October 1st before gradually intensifying over the SCS. It reached its maximum intensity of ~50 m/s at ~10:00 a.m. on October 4th. The BHOT recorded the maximum wind speed of ~30 m/s at 9:00 a.m. All the time in this study referred to Beijing Time (UTC+8). Mujigae made landfall at Zhanjiang of Guangdong and gradually weakened after. BHOT was located on the right side of Mujigae during the TC passage (Figure 1). Our study focused on the period from 12:00 a.m. on October 3rd to 12:00 a.m. on October 5th when the typhoon passed by the BHOT.

The wind speed and direction, the air and sea surface skin temperature, and the distance and azimuth from BHOT to the typhoon center during this focused period were presented in Figure 2. Notably, the azimuth of BHOT was relative to the moving direction of TC at each time, and the sea surface skin temperature was measured by a precision infrared radiometer mounted on the tower at roughly the same height as eddy covariance system. The distance from BHOT to the TC center gradually decreased from 460 km at 12:00 a.m. on October 3rd, and the minimum was about 72 km at 11:00 a.m. on October 4th, then the TC gradually moved away from the BHOT (Figure 2c). At around 11:00 a.m., BHOT located in the near field of Mujigae according to the distinguished method proposed by Holthuijsen et al. (2012). However, the wind speed was not the maximum at 11:00 a.m., the maximum wind speed with ~29 m/s appeared at 9:00 a.m., and the wind speed changed little from 9:00 to 11:00 a.m. (Figure 2a). The azimuth of BHOT relative to the moving direction of TC was greater than zero during the selected period. At 11:00 a.m., BHOT nearly located in the east of TC, and then shifted from the right front quadrant to the right rear quadrant of TC. Meanwhile, the wind direction changed from north-northeast to southeast (Figure 2a). The sea surface skin temperature was generally slightly greater than air temperature, however, the maximum difference was ~1°C (Figure 2b). Additionally, the *Rib* was calculated based on the bulk Richardson number (*Rib*) method (Sharana et al., 2005). *Rib* generally ranged from 0.01 to −0.04, which indicated that the atmospheric stratification was nearly neutral (Bi et al., 2005).

Typhoon Rammasun passed through the observation site during the ocean turbulence experiment from 13 to 21 July 2014 (Ma et al., 2020; Qiao et al., 2016), and the maximum wind speed of ~25 m/s was recorded. During this experiment, a bottom-mounted acoustic wave buoy (acoustic wave and current profiler, AWAC, Nortek, 1 MHz) was used to observe the surface wave. The wave height, period and direction were recorded by the wave buoy at

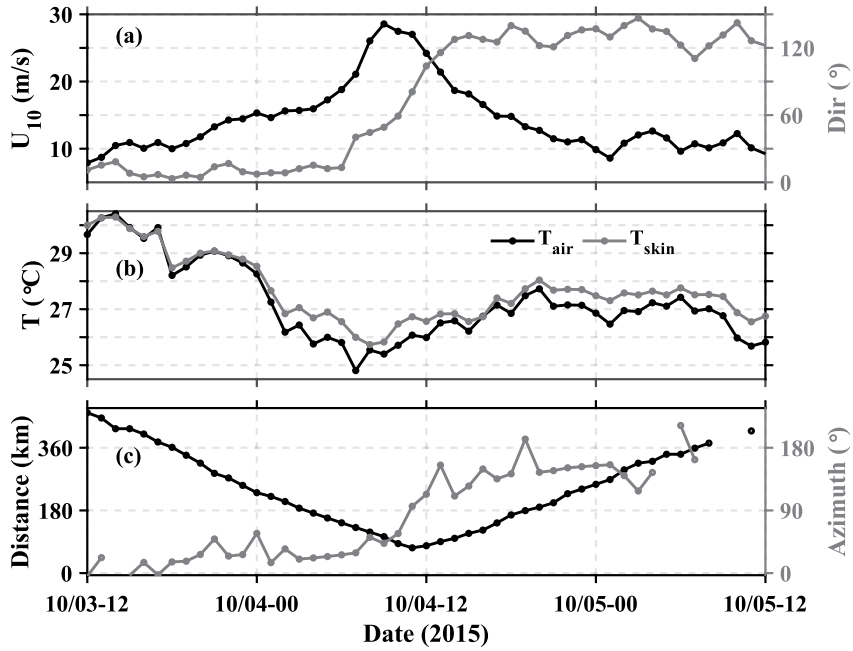

Figure 2. Time series of wind speed U_{10} and wind direction (a), and the air and sea surface skin temperatures (b) recoded at BoHe observational tower (BHOT) site, and the distance and the azimuth from BHOT site to typhoon center (c) during the focused period during Typhoon Mujigae. The black and gray dotted lines represent U_{10} and wind direction in (a), and air and sea surface skin temperature in (b), and distance and azimuth in (c), respectively.

a time interval of 30 min. The sampling frequency of the wave buoy was set to 2 Hz. The precision is less than 1% of the measurement range for wave height, it is 2° for wave direction. The range of wave period is 0.5–100 s. The resolution is 1 cm for wave height and 0.1° for direction. The wave buoy was overturned by the typhoon after 9:30 on July 18th, the direction and period information of surface waves became invalid. Fortunately, the pressure sensors of wave buoy recorded the wave height information. More details can be found in Qiao et al. (2016) and Ma et al. (2020). In the current study, the significant wave height, the peak wave period, and the mean wave direction were used to analyze and validate the fifth generation ECMWF reanalysis product (ERA5 reanalysis).

The ERA5 reanalysis product consists of atmospheric, ocean-wave and land-surface quantities from 1950 to present. This data set has the resolution of 0.25° for the reanalysis, including the hourly output on both pressure and single levels. More information can be accessible in the Climate Data Store website. The hourly product on single level was used in this study. According to the latitude and longitude of BHOT, the ERA5 data in latitude and longitude range from 20° to 21.5°N and 111° to 112.5°E were selected to interpolate to BHOT site using a cubic spline interpolation method. During Typhoon Mujigae, the wind speed and direction, the mean wave direction and peak wave phase speed were used to study the wave situation and its potential linkage to the drag coefficient. During Typhoon Rammasun, the wind and wave products were used to compare with observations.

3. Results and Discussions

3.1. Comparison Between ERA5 and Observations

Observations of the wind speed, wind direction and surface wave elements during Typhoon Rammasun at the BHOT site were used to verify the ERA5 reanalysis, as shown in Figure 3. The correlation coefficients for wind speed, wind direction, significant wave height, wave direction and peak wave period between ERA5 and observations were 0.96, 0.91, 0.90, 0.97, and 0.78, respectively, all of which were statistically significant at a confidence level of 95%. The differences were negligible for U_{10}, since the root mean square error (RMSE) was 0.1 m/s. The time tendency of wind speed was basically the same between ERA5 and observations. The maximum wind speed in ERA5 was smaller than that in observations by ~4 m/s (Figure 3a), probably due to the limited resolution of ERA5. The wind direction from ERA5 had a systematic bias of 20° against the observations. While the wave directions deviated from the observations with a RMSE of 25° (Figure 3b). The significant wave heights from

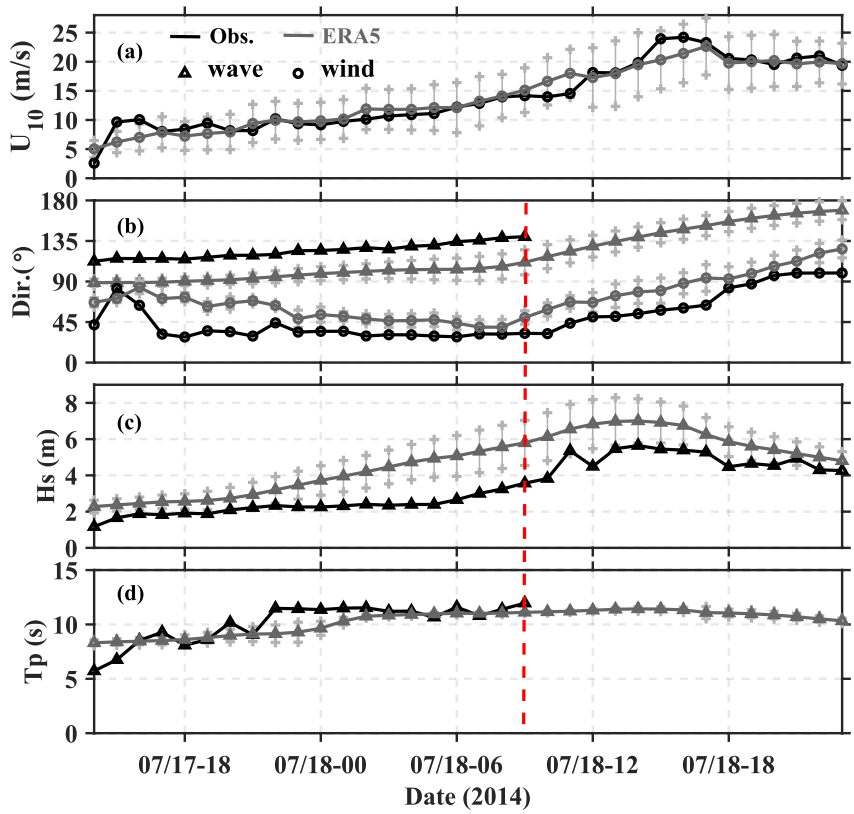

Figure 3. Comparisons between ERA5 reanalysis data and observations for the wind speed (a), and wind and mean wave direction (b), and significant wave height H_s (c), and peak wave period T_p (d) during Typhoon Rammasun in 2014. The black and gray lines with circle or triangle refer to the observation and ERA5, respectively. The red dashed line represents the end time of wave direction and wave period. The standard error bars (gray plus) of ERA5 are shown in the plots. Here, the standard deviation is calculated from 16 grid points of ERA5 near the observational site.

ERA5 were larger than the observations and the RMSE was 1.3 m (Figure 3c). The overestimation of wave height from ERA5 was also reported by Kumar et al. (2020). The differences in the peak wave period between ERA5 and observations were small. The RMSE was 0.3 s (Figure 3d). Although there were some differences between ERA5 and observations, the shifting trend of ERA5 was quite similar to that of observations for both wind and wave. The above comparisons indicated a reasonable agreement between ERA5 and observations. Many previous studies analyzed the reliability of ERA5 against observations and concluded that the ERA5 can resolve the TC induced winds and waves (Bian et al., 2021; Dullaart et al., 2020; Kumar et al., 2020).

Next, the wind between ERA5 and observations during Typhoon Mujigae were compared. Because ERA5 did not provide the best track of TC, we determined the TC center at each moment through the wind field data from ERA5, and then provided the best track. Figure 4a showed the 10 m wind speed from ERA5. The first step was to determine the maximum wind speed and then find the location of the minimum wind speed near the maximum, which was defined as the TC center. Figure 4b compared the track of Mujigae derived from ERA5 and the best track, showing good agreement. The comparison of wind speed and direction during Mujigae were basically consistent with those during Rammasun. Both wind speed and direction in ERA5 captured the time variation as in observations. The differences in wind speed were small (<2 m/s) during the interested period except the maximum wind was not captured by ERA5 (Figure 5a). Therefore, the wave direction from ERA5 was used to quantitively describe the wave situations during Mujigae. In the right front quadrant of the TC (before 11:00 a.m. on October 4th), the deviations between wave direction and wind direction were mostly in the range of 45°–90°. From 7:00 a.m. to 11:00 a.m. the direction difference gradually decreased to approximately 30°. With the northwestward movement of the TC, the BHOT shifted from the right front to the right rear quadrant of the TC where the wave was nearly aligned with the wind direction (Figure 5b). Following the definition of Holthuijsen et al. (2012), the wave state was categorized as cross swell in the right front quadrant and as following swell or

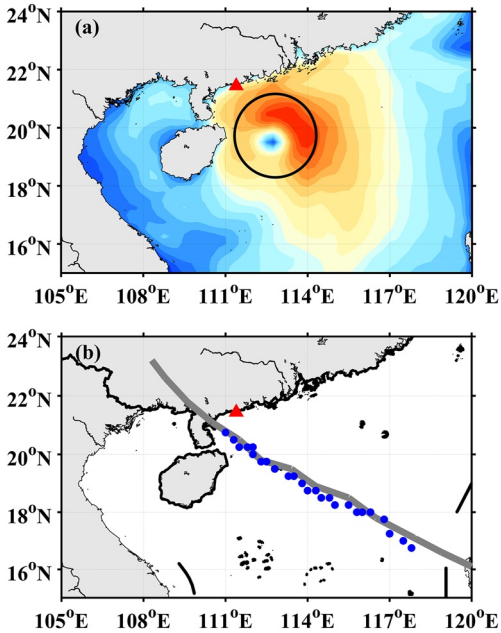

Figure 4. The wind field of ERA5 at 23:00 on October 3rd (a) and the best track of Typhoon Mujigae (b). The blue dots represent the tropical cyclone (TC) center derived from the wind field of ERA5 in (b). The location with minimum wind speed in the black circle in (a) is defined as the TC center, and the track points with clear TC center after TC entering the South China Sea are shown in (b).

wind sea in the right rear quadrant of Typhoon Mujigae, which was similar to the results of Holthuijsen et al. (2012) and Liu et al. (2017).

3.2. Relationship Between Drag Coefficient and Wind Speed

The relationship between C_D and the wind speed U_{10} for all data was shown in Figure 6. The black line presented the mean C_D with U_{10} interval of 3 m/s and the error bars (Figure 6). It was evident that C_D decreased with the increase of U_{10} at low wind speeds ($U_{10} < 5\,m/s$), and then increased with U_{10} at moderate wind speeds ($5\,m/s < U_{10} < 20\,m/s$). When the wind speed approached 20 m/s, the mean drag coefficient reached a peak value ($C_D \approx 3 \times 10^{-3}$) and then decreased with the further increase of wind speed. The minimum and maximum values of C_D were approximately 2×10^{-3} and 4×10^{-3} at this critical wind speed for C_D saturation.

Figure 7a presented the comparison of C_D between our observations and previous studies. Only the mean values of C_D were shown, the error bars were absent. The symbols shown in Figure 7a represent the average over a certain wind speed interval, such as 3 m/s in our study. The critical wind speeds U_{10c} for C_D saturation from different observational locations with C_D observed or estimated using various approaches were summarized in Figure 7b, which was for statistical characteristics of C_D at high wind speeds in different water depths. Here, we grouped U_{10c} into three groups: coastal region, continental shelf and open ocean based on the water depths. The variation of C_D with wind speed recorded on BHOT was consistent with that of previous studies at low to moderate wind speeds (3–18 m/s) (Vickers et al., 2013; Zhao et al., 2015).

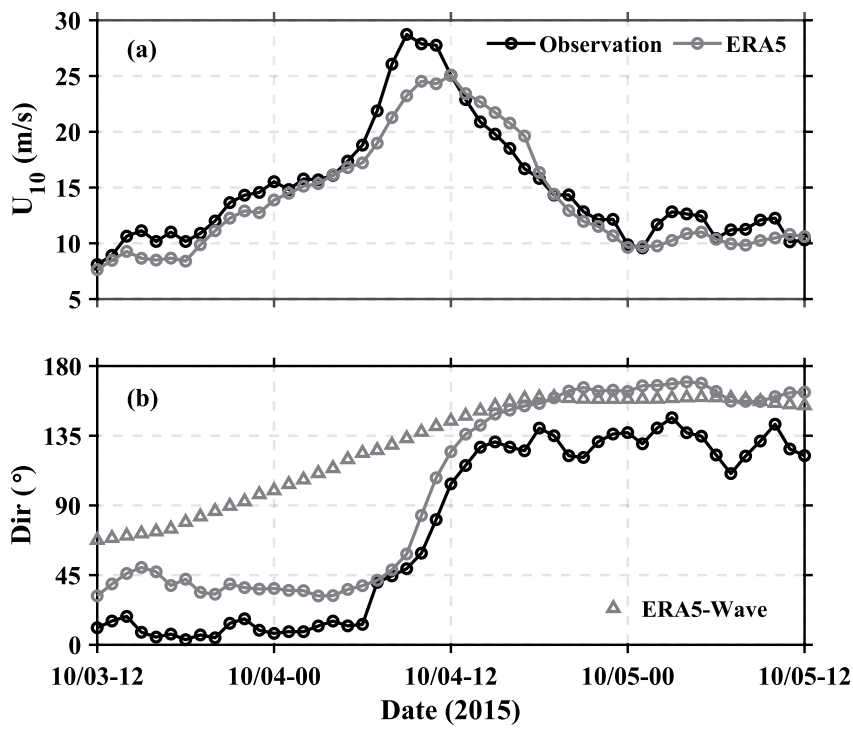

Figure 5. Comparisons between ERA5 reanalysis data and observations for the wind speed (a) and wind direction (b) at selected period during Typhoon Mujigae. The black and gray lines with circles refer to the observation and ERA5, respectively. In (b), the wave direction from the ERA5 reanalysis is also shown (gray triangle).

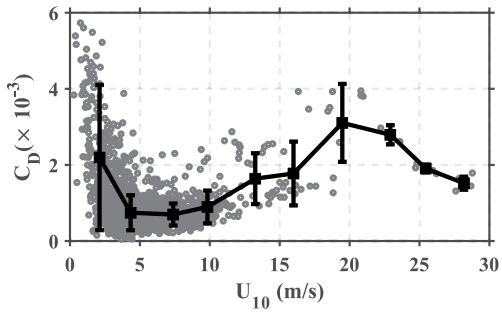

Figure 6. The variation of drag coefficient C_D with wind speed U_{10} during the observational period. The rectangle represents the mean value of C_D with wind speed bin size of 3 m/s. Standard error bars are also shown.

For coastal regions, the observed C_D values during Typhoon Mujigae were similar to those observed over the Pacific coast ocean presented by Vickers et al. (2013), including the overall variation with wind speed and the U_{10c} of approximately 20 m/s (Figures 7a and 7b). Furthermore, our results were compared with estimates in two other typhoons given by Bi et al. (2015) and Zhao et al. (2015). Our U_{10c} (~20 m/s) was larger than that (~18 m/s) presented in Bi et al. (2015), but was smaller than that (~24 m/s) of Zhao et al. (2015). Bi et al. (2015) used the same method as ours, while Zhao et al. (2015) used the wind profile method to estimate C_D. The high wind data used by Bi et al. (2015) was mainly from the Typhoon Nesat in 2011, which was further away from the BHOT site than Typhoon Mujigae. This probably brought slight difference of U_{10c} against ours. The difference with the result of Zhao et al. (2015) was probably caused by different methods and wave states.

Despite of different observing strategies and analysis methods, U_{10c} is statistically significantly different between coastal region and open ocean. The mean U_{10c} is ~20 m/s over coastal regions, while it is ~30 m/s over open oceans. This difference might be associated with different wave state under various water depths. In shallow water, the surface waves are more likely to be broken such that the sea spray coverage increases. The enhanced spray stress would in turn reduce the drag coefficient (Andreas, 2004). Besides, the wind waves decay faster in shallow water due to the wave breaking and the bottom friction effect. Under this situation, the wind stress varies with the wind speed in a significantly different way relative to that over the deep water (Chen, Ginis, & Hara, 2020; Takagaki et al., 2016). Xu and Yu (2021) simulated the variations of drag coefficient with water depth by considering the effects of water depth on the wind wave and the sea spray using an atmospheric wave

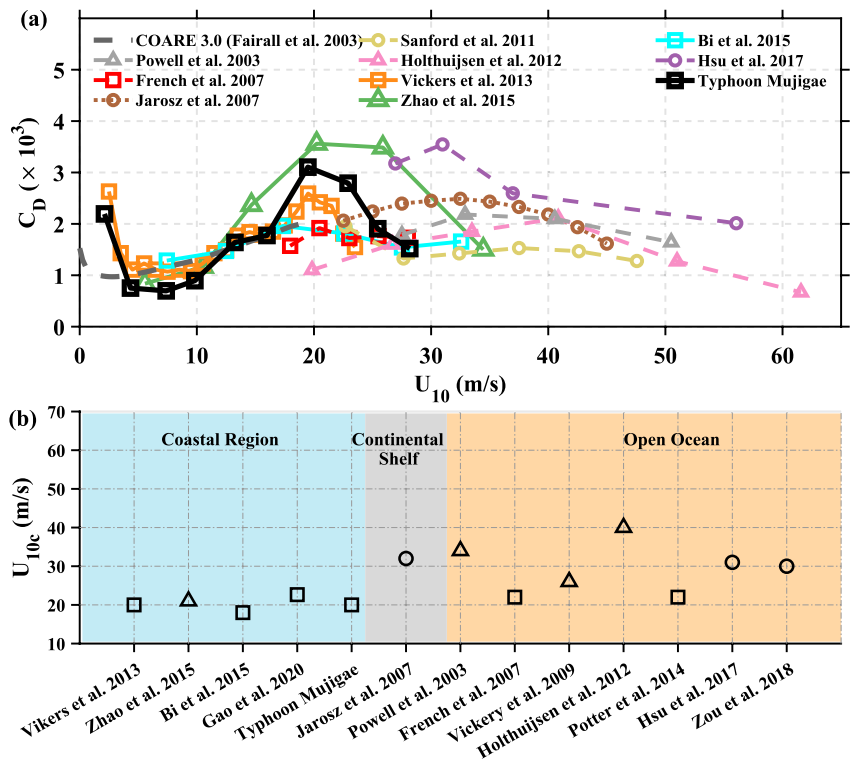

Figure 7. The relationship between mean drag coefficient C_D and wind speed U_{10} (a) for observations during Typhoon Mujigae (black solid line with rectangle). Previous observational results are also shown to compare with our result. In (a), solid lines, dotted lines, and dashed lines represent coastal region, continental shelf and open ocean, respectively. The critical wind speed U_{10c} for C_D saturation given by different investigations are shown in (b). In both plots, different symbols in lines represent different data collection or process methods. Rectangle, circle and triangle represent eddy covariance, bottom-up momentum balance and semi-logarithmic wind profile method, respectively.

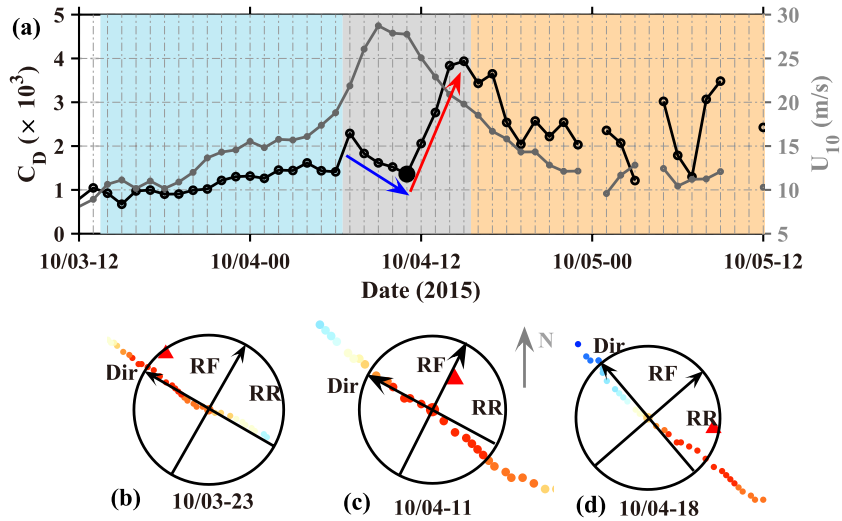

Figure 8. Time series of the drag coefficient C_D (black line with circle) and U_{10} (gray line) during the focused periods (a). Periods A, B, and C represent the period when U_{10} increases from approximately 10 m/s to 20 m/s before typhoon, and that when U_{10} is greater than 20 m/s during typhoon, and that when U_{10} decreases from approximately 20 m/s to 10 m/s, respectively. The blue and red arrows indicate the downward and upward trend of C_D during Period B. Plots (b, c, and d) present the BoHe observational tower's (BHOT's) location in different quadrants of typhoon at a specific time during Periods A, B, and C, which shows the shift in the typhoon quadrant for the BHOT site.

boundary layer model. Although their simulated U_{10c} is slightly larger than our observations in the similar water depths, the difference of U_{10c} in different water depths is consistent with our statistical result.

3.3. Spatial Distribution of Drag Coefficient

Three sub-periods (Periods of A, B, and C in Figure 8a, hereafter, P-A, P-B, P-C) according to the wind speed variation with time were used to investigate the spatial distribution of the drag coefficient. P-A and P-C represented the time periods when the wind speeds were less than 20 m/s in the rising and falling stage of wind speed, respectively. P-B represented the time periods when the wind speeds were greater than 20 m/s. The drag coefficient C_D in P-A was much lower than that in P-C, with an average of 1.2×10^{-3} in P-A and 2.5×10^{-3} in P-C. Both periods had basically the same wind speed range (10 m/s < U_{10} < 20 m/s), however, observations during these two periods were at two different quadrants of the TC, P-A represented the right front quadrant and P-C represented the right rear quadrant (Figures 8b and 8d). During P-B, the wind speed exceeded 20 m/s, and C_D decreased with the increase of wind speed. However, its value before 11:00 a.m. on October 4th was less than that after this time. At 11:00 a.m., the typhoon center was closest to the platform (Figure 2c), and BHOT was nearly in the east to the motion direction of TC (Figure 8c), however, C_D had a minimum value of $\sim 1.4 \times 10^{-3}$ at this time when the wind speed was ~28 m/s. Mujigae continued to move northwest and was further away from BHOT. At 15:00 a.m., C_D increased to the maximum, $\sim 4 \times 10^{-3}$ when the wind speed was ~20 m/s. The behavior of C_D during P-B indicated that the C_D varied significantly with the azimuthal location relative to the TC center.

Figure 9 showed the behaviors of observed U_{10} and C_D, the wave off wind angle θ and the wave age ($C_p/U_{10}\cos(\theta)$, where C_p is the peak wave phase speed) derived from ERA5 in the motion-relative quadrants. Although the wind speeds were symmetric at a given radius in the right rear and right front quadrants (Figure 9a), the drag coefficient C_D presented an asymmetry in these two quadrants (Figure 9b). C_D in the right rear quadrant was much larger than that in the right front quadrant, which was similar to the results derived from the wind profiles in the rear and right front quadrants over the open ocean reported by Holthuijsen et al. (2012). However, the differences from our study were that their wind speeds were greater than 20 m/s and they did not present the spatial distribution of C_D. The different behaviors of C_D between the two quadrants studied here were possibly dependent on the difference in wave state (Figures 9c and 9d).

In the right front quadrant of TC, swells generated by the TC cross the local wind-wave. Under this situation, the energy of wind-wave is probably reduced by swells (Chen, Ginis, & Hara, 2020; García-Nava et al., 2012). Since

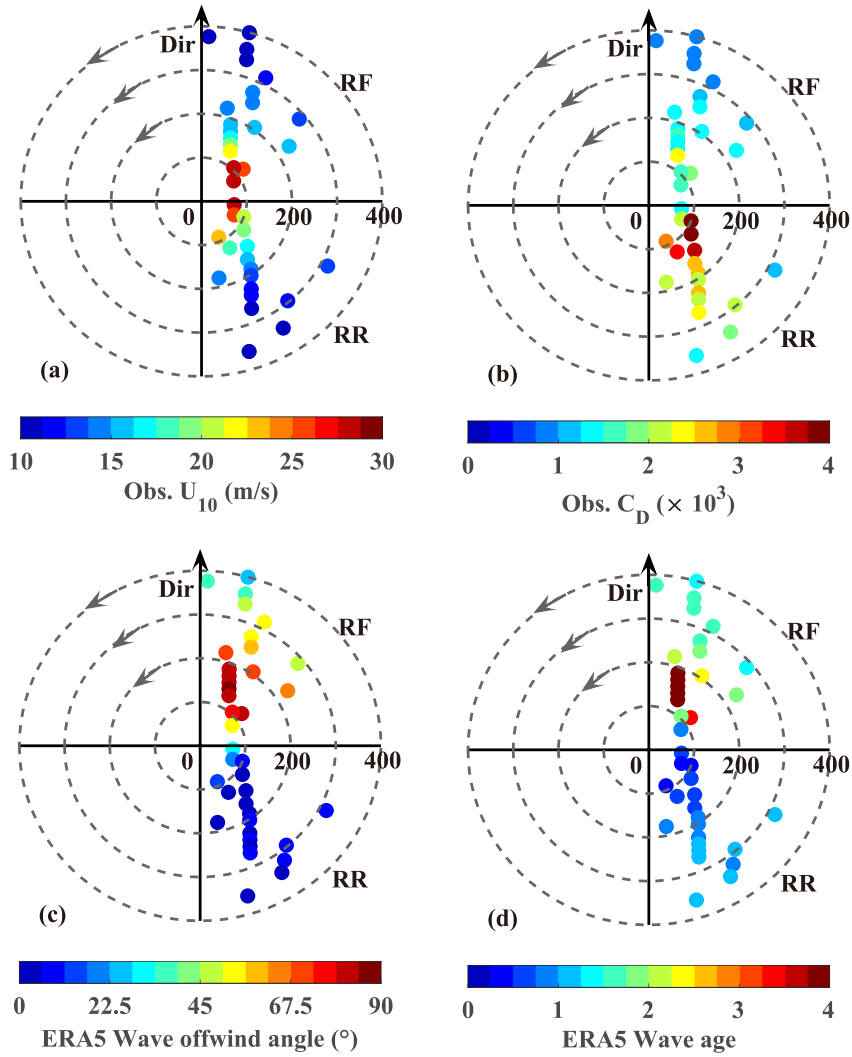

Figure 9. The distributions of wind speed U_{10} (a) and drag coefficient C_D(b) from observations, and the distributions of the angle between wind and wave direction (c), and the wave age (d) from ERA5 reanalysis in the motion-relative quadrants. The black arrows in all plots represent the moving direction of tropical cyclone (TC) and the gray arrows represent the rotation direction of TC. RF and RR represent the right front and right rear quadrants. The circle from inside to outside refers to the distance from the typhoon center, from 0 to 400 km with interval of 100 km. The colored dots in all plots represent the location of observational site relative to the typhoon center.

wind-wave supports most of the total wind stress, the reduced wind-wave is likely responsible for the lower C_D in the right front quadrant. The laboratory results of Takagaki et al. (2016) also showed that the attenuation of the wind-wave spectrum can lead to the saturation of C_D. In the right rear quadrant of the TC during landfall, the wave direction was generally aligned with the wind direction (Figures 5b and 9c). The long fetch allowed for the development of wind-wave, which in turn enhanced C_D. Chen, Ginis, and Hara (2020) attributed this enhancement to the shoaling wave effect. Furthermore, the wave age in the right front quadrant was larger than that in the right rear quadrant, which was another factor that affects the wind stress. Drennan et al. (2003) showed that the larger wave age causes smaller C_D (see their Figure 10), which supported our finding. The sea spray also affects the wind stress magnitude (Andreas, 2004; Holthuijsen et al., 2012; Zhao et al., 2006). Sea spray typically reduces the drag coefficient at high wind speeds. However, evaluation of sea spray effect on the drag coefficient is beyond the scope of this study because of no information on sea spray. This study focused on the wave effects using the ERA5 reanalysis to qualitatively determine the wave field which had limitations in TC conditions. Further work requires specially designed field experiment to collect flux and wave observations in TCs to verify the findings in this study.

4. Conclusions

The momentum flux over the coastal region during Typhoon Mujigae in 2015 was measured on an offshore platform in the northern SCS. Results showed that the characteristic of C_D in the right front and right rear quadrants of the TC is quite different, C_D in the latter is much larger than that in the former. At higher wind speeds than 20 m/s, C_D had a minimum value when the observational site was closest to the typhoon center. After the landfall time, C_D reached its maximum. This result suggested that the C_D varies significantly with the location/distance relative to the typhoon center. The variations of wave state in different quadrants of the TC may lead to the enhancement or reduction of C_D at the same wind speed. Additionally, observations confirmed the drag coefficient C_D over coastal region reached a peak value at the wind speed of approximately 20 m/s and then decayed with the wind speed. This critical wind speed for C_D saturation was much lower than that (~30 m/s) over the open ocean.

Due to the lack of the surface wave observations, the wave elements from ERA5 reanalysis were used to estimate the wave field during the passage of Mujigae. Although ERA5 shows a good agreement with observations at BHOT site, field experiments with collocated flux, wave and sea spray observations in TCs are needed to further understand the asymmetric behavior of the drag coefficient and its relationship to the sea state and sea spray distribution. Results provided the first direct observations of the asymmetry of drag coefficient in the right front and right rear quadrants of a TC over the coastal region. The uniform drag coefficients in different quadrants may cause the TC model to overestimate and underestimate the typhoon intensity in the right rear and right front quadrants, which may be one of the potential reasons for the bottleneck on typhoon intensity forecasting. Therefore, this asymmetry should be considered in TC forecast models.

Data Availability Statement

ERA5 data can be found in https://doi.org/10.24381/cds.adbb2d47. Data used in this study can be accessible in https://doi.org/10.17632/sj776jbk7m.3.

Acknowledgments
This research was financially supported by the Marine S&T Fund of Shandong Province for Pilot National Laboratory for Marine Science and Technology (Qingdao) under Grants 2022QNLM010102, Basic Scientific Fund for National Public Research Institutes of China under Grants 2022Q01, National Natural Science Foundation of China under Grants 41821004, and 42276024. Jun A. Zhang was supported by NOAA Grants NA14NWS4680028, NA21OAR4590370, and NOAA NA19OAR0220186, and NSF grant AGS-1822128. We are grateful to the reviewers who provided comments and suggestions that helped substantially improve our paper.

References

Andreas, E. L. (2004). Spray stress revisited. *Journal of Physical Oceanography*, *34*(6), 1429–1440. https://doi.org/10.1175/1520-0485(2004)034<1429:SSR>2.0.CO;2

Bell, M. M., Montgomery, M. T., & Emanuel, K. A. (2012). Air-sea enthalpy and momentum exchange at major Hurricane wind speeds observed during CBLAST. *Journal of the Atmospheric Sciences*, *69*(11), 3197–3222. https://doi.org/10.1175/JAS-D-11-0276.1

Bi, X., Gao, Z., Liu, Y., Liu, F., Song, Q., Huang, J., et al. (2015). Observed drag coefficients in high winds in the near offshore of the South China Sea. *Journal of Geophysical Research: Atmospheres*, *120*(13), 6444–6459. https://doi.org/10.1002/2015JD023172

Bi, X., Liu, F., & Wu, D. (2005). Comparison of some limits for stability classification. *Journal of Tropical Meteorology*, *11*(2), 161–168. https://doi.org/10.1360/biodiv.050028

Bian, G. F., Nie, G. Z., & Qiu, X. (2021). How well is outer tropical cyclone size represented in the ERA5 reanalysis dataset? *Atmospheric Research*, *249*, 105339. https://doi.org/10.1016/j.atmosres.2020.105339

Black, P. G., D'Asaro, E. A., Drennan, W. M., French, J. R., Niiler, P. P., Sanford, T. B., et al. (2007). Air-sea exchange in hurricanes: Synthesis of observations from the coupled boundary layer air-sea transfer experiment. *Bulletin of the American Meteorological Society*, *88*(3), 357–374. https://doi.org/10.1175/BAMS-88-3-357

Chen, S., Qiao, F., Huang, C. J., & Zhao, B. (2018). Deviation of wind stress from wind direction under low wind conditions. *Journal of Geophysical Research: Oceans*, *123*(12), 9357–9368. https://doi.org/10.1029/2018JC014137

Chen, S., Qiao, F., Jiang, W., Guo, J., & Dai, D. (2019). Impact of surface waves on wind stress under low to moderate wind conditions. *Journal of Physical Oceanography*, *49*(8), 2017–2028. https://doi.org/10.1175/JPO-D-18-0266.1

Chen, S., Qiao, F., Xue, Y., Chen, S., & Ma, H. (2020). Directional characteristic of wind stress vector under swell-dominated conditions. *Journal of Geophysical Research: Oceans*, *125*(7), e2020JC016352. https://doi.org/10.1029/2020JC016352

Chen, X., Ginis, I., & Hara, T. (2020). Impact of shoaling ocean surface waves on wind stress and drag coefficient in coastal waters: 2. Tropical cyclones. *Journal of Geophysical Research: Oceans*, *125*(7), e2020JC016223. https://doi.org/10.1029/2020JC016223

Donelan, M. A., Haus, B. K., Reul, N., Plant, W. J., Stiassnie, M., Graber, H. C., et al. (2004). On the limiting aerodynamic roughness of the ocean in very strong winds. *Geophysical Research Letters*, *31*(18), 355–366. https://doi.org/10.1029/2004GL019460

Drennan, W. M., Graber, H. C., Hauser, D., & Quentin, C. (2003). On the wave age dependence of wind stress over pure wind seas. *Journal of Geophysical Research*, *108*(C3), 2062. https://doi.org/10.1029/2000JC000715

Dullaart, J. C., Muis, S., Bloemendaal, N., & Aerts, J. C. (2020). Advancing global storm surge modelling using the new ERA5 climate reanalysis. *Climate Dynamics*, *54*(1), 1007–1021. https://doi.org/10.1007/s00382-019-05044-0

Edson, J. B., Jampana, V., Weller, R., Bigorre, S., Plueddemann, A. J., Fairall, C., et al. (2013). On the exchange of momentum over the open ocean. *Journal of Physical Oceanography*, *43*(8), 1589–1610. https://doi.org/10.1175/JPO-D-12-0173.1

Emanuel, K. A. (1995). Sensitivity of tropical cyclones to surface exchange coefficients and a revised steady-state model incorporating eye dynamics. *Journal of the Atmospheric Sciences*, *52*(22), 3969–3976. https://doi.org/10.1175/1520-0469(1995)052<3969:SOTCTS>2.0.CO;2

Fairall, C. W., Bradley, E. F., Hare, J. E., Grachev, A. A., & Edson, J. B. (2003). Bulk parameterization of air-sea fluxes: Updates and verification for the COARE algorithm. *Journal of Climate*, *16*(4), 571–591. https://doi.org/10.1175/1520-0442(2003)016<0571:BPOASF>2.0.CO;2

French, J. R., Drennan, W. M., Zhang, J. A., & Black, P. G. (2007). Turbulent fluxes in the hurricane boundary layer. Part I;: Momentum flux. *Journal of the Atmospheric Sciences*, *64*(4), 1089–1102. https://doi.org/10.1175/JAS3887.1

García-Nava, H., Ocampo-Torres, F. J., Hwang, P. A., & Osuna, P. (2012). Reduction of wind stress due to swell at high wind conditions. *Journal of Geophysical Research*, *117*(5), 1–11. https://doi.org/10.1029/2011JC007833

Holthuijsen, L. H., Powell, M. D., & Pietrzak, J. D. (2012). Wind and waves in extreme hurricanes. *Journal of Geophysical Research*, *117*(C9), 1–15. https://doi.org/10.1029/2012JC007983

Hsu, J. Y., Lien, R. C., D'Asaro, E. A., & Sanford, T. B. (2017). Estimates of surface wind stress and drag coefficients in typhoon Megi. *Journal of Physical Oceanography*, *47*(3), 545–565. https://doi.org/10.1029/2012JC007983

Jarosz, E., Mitchell, D. A., Wang, D. W., & Teague, W. J. (2007). Bottom-up determination of air-sea momentum exchange under a major tropical cyclone. *Science*, *315*(5819), 1707–1709. https://doi.org/10.1126/science.1136466

Kumar, V. S., George, J., & Joseph, D. (2020). Hourly maximum individual wave height in the Indian shelf seas—Its spatial and temporal variations in the recent 40 years. *Ocean Dynamics*, *70*(10), 1283–1302. https://doi.org/10.1007/s10236-020-01395-z

Large, W. G., & Pond, P. (1981). Open ocean momentum flux measurements in moderate to strong winds. *Journal of Physical Oceanography*, *11*(3), 324–336. https://doi.org/10.1175/1520-0485(1981)0112.0.CO;2

Liu, Q., Babanin, A., Fan, Y., Zieger, S., Guan, C., & Moon, I. J. (2017). Numerical simulations of ocean surface waves under hurricane conditions: Assessment of existing model performance. *Ocean Modelling*, *118*, 73–93. https://doi.org/10.1016/j.ocemod.2017.08.005

Ma, H., Dai, D., Guo, J., & Qiao, F. (2020). Observational evidence of surface wave-generated strong ocean turbulence. *Journal of Geophysical Research: Oceans*, *125*(2), e2019JC015657. https://doi.org/10.1029/2019JC015657

Moon, I. J., Ginis, I., & Hara, T. (2004). Effect of surface waves on Charnock coefficient under tropical cyclones. *Geophysical Research Letters*, *31*(20), 379–398. https://doi.org/10.1029/2004GL020988

Potter, H., Collins, C. O., III., Drennan, W. M., & Graber, H. C. (2015). Observations of wind stress direction during typhoon Chaba (2010). *Geophysical Research Letters*, *42*(11), 9898–9905. https://doi.org/10.1002/2015GL065173

Powell, M. D., Vickery, P. J., & Reinhold, T. A. (2003). Reduced drag coefficient for high wind speeds in tropical cyclones. *Nature*, *422*(6929), 279–283. https://doi.org/10.1038/nature01481

Qiao, F., Yuan, Y., Deng, J., Dai, D., & Song, Z. (2016). Wave–turbulence interaction-induced vertical mixing and its effects in ocean and climate models. *Philosophical Transactions of the Royal Society A: Mathematical, Physical & Engineering Sciences*, *374*(2065), 20150201. https://doi.org/10.1098/rsta.2015.0201

Reichl, B. G., Hara, T., & Ginis, I. (2014). Sea state dependence of the wind stress over the ocean under hurricane winds. *Journal of Geophysical Research: Oceans*, *119*(1), 30–51. https://doi.org/10.1002/2013JC009289

Sanford, T. B., Price, J. F., & Girton, J. B. (2011). Upper-ocean response to hurricane Frances (2004) observed by profiling EM-APEX Floats*. *Journal of Physical Oceanography*, *41*(6), 1041–1056. https://doi.org/10.1175/2010JPO4313.1

Sharana, M., Rama Krishna, T. V. B. P. S., & Panda, J. (2005). Relations among stability parameters in the stable surface layer: Golder curves revisited. *Atmospheric Environment*, *39*(30), 5619–5623. https://doi.org/10.1016/j.atmosenv.2005.05.034

Takagaki, N., Komori, S., Suzuki, N., Iwano, K., & Kurose, R. (2016). Mechanism of drag coefficient saturation at strong wind speeds. *Geophysical Research Letters*, *43*(18), 9829–9835. https://doi.org/10.1002/2016GL070666

Vickers, D., Mahrt, L., & Andreas, E. L. (2013). Estimates of the 10-m neutral sea surface drag coefficient from aircraft eddy-covariance measurements. *Journal of Physical Oceanography*, *43*(2), 301–310. https://doi.org/10.1175/JPO-D-12-0101.1

Xu, Y., & Yu, X. (2021). Enhanced atmospheric wave boundary layer model for evaluation of wind stress over waters of finite depth. *Progress in Oceanography*, *198*, 102664. https://doi.org/10.1016/j.pocean.2021.102664

Zhao, D., Toba, Y., Sugioka, K., & Komori, S. (2006). New sea spray generation function for spume droplets. *Journal of Geophysical Research*, *111*(C2), C02007. https://doi.org/10.1029/2005JC002960

Zhao, Z. K., Liu, C. X., Li, Q., Dai, G. F., Song, Q. T., & Lv, W. H. (2015). Typhoon air-sea drag coefficient in coastal regions. *Journal of Geophysical Research: Oceans*, *120*(2), 716–727. https://doi.org/10.1002/2014JC010283